

## Recent advances in imaging systems and photonic nanostructures inspired by insect eye geometry

Gil Ju Lee, Young Jin Yoo & Young Min Song

To cite this article: Gil Ju Lee, Young Jin Yoo & Young Min Song (2018) Recent advances in imaging systems and photonic nanostructures inspired by insect eye geometry, Applied Spectroscopy Reviews, 53:2-4, 112-128, DOI: [10.1080/05704928.2017.1324469](https://doi.org/10.1080/05704928.2017.1324469)

To link to this article: <https://doi.org/10.1080/05704928.2017.1324469>



Published online: 24 May 2017.



Submit your article to this journal [↗](#)



Article views: 420



View related articles [↗](#)




View Crossmark data [↗](#)



Citing articles: 8 View citing articles [↗](#)



## Recent advances in imaging systems and photonic nanostructures inspired by insect eye geometry

Gil Ju Lee , Young Jin Yoo, and Young Min Song

School of Electrical Engineering and Computer Science, Gwangju Institute of Science and Technology, Gwangju, Republic of Korea

### ABSTRACT



Studying sensory light in nature provides opportunities for the development of new types of imaging systems and optical components that cannot be achieved with existing technologies. Insect eyes, i.e., compound eyes, are particularly notable for their exceptional optical characteristics, such as wide fields of view, nearly infinite depth-of-field, and high sensitivity to motion. The construction of manmade compound eye imagers with these characteristics is of significant interest due to their strong potential for various applications, including surveillance, security, and bio-medical devices. Furthermore, night-active insects have nanophotonic structures that provide exceptional optical behaviors (e.g., broadband antireflection of light), which are beneficial for applications in high-efficiency optoelectronic devices. In this review, recent progress is reviewed for optical devices and optical imaging systems with designs inspired by the geometry of insect eyes. The design guidelines and fabrication issues are also discussed.

### KEYWORDS

Applications; bio-inspired imaging system; biomimicry; compound eye; instrumentation

## Introduction

Animal vision is critical in their survival through locating food, navigating, and identifying mating suitability. Currently, biological image-capturing optical systems are attracting significant interest among scientists and engineers due to their sophisticated structures and functionalities. Biological eyes have exhibited remarkable structural complexity that integrates distinct components across many length scales, from nanometer to centimeter. The functionality results from the organization of the functional molecules, cells, and other biomaterials. There are numerous examples of vision systems that offer high visual acuity, high sensitivity to motion, excellent photosensitivity in low-light environments, wide fields of view (FOVs), polarization perception enhancement, aberration correction, and near infinite depth-of-field (1–7). The diversity of visual systems found in nature provides a variety of design options with desirable operational properties, particularly compared with the designs found in conventional imaging systems.

**CONTACT** Young Min Song  [ymsong@gist.ac.kr](mailto:ymsong@gist.ac.kr)  School of Electrical Engineering and Computer Science, Gwangju Institute of Science and Technology, 123 Cheomdan-gwagiro, Buk-gu, Gwangju 61005, Republic of Korea.

Color versions of one or more figures in this article are available online at [www.tandfonline.com/laps](http://www.tandfonline.com/laps).

© 2018 Taylor & Francis Group, LLC

Much like conventional imaging technologies, biological eyes can be described as an integrated set of front-end primary optics (i.e., the optical components that collect and direct light) and a back-end processor (i.e., the components that capture and process the collected visual information), as well as additional optical components that improve the overall system function. The structures of most animal eyes can be described as a variation of one of approximately eight to ten major eye structures, and these are commonly categorized into two major eye types (6, 7): single lens eyes and compound eyes. Single lens (or camera-type) eyes have a single integrated lens system that focuses incoming light onto common photoreceptors in the back-end structure. In contrast, compound eyes have multiple lenses per eye. Improved understanding of the light-sensing organs in biology reveals that the compound eyes of arthropods are particularly notable for their exceptionally wide fields of view, high sensitivity to motion, and nearly infinite depth-of-field. It is also found that nocturnal insects have tapered nanostructures on the surface of their cornea for broadband antireflection of incoming light. Mimicking the compound eyes with these characteristics has been of long-standing interest due to their potential for use in numerous industrial applications. This review begins by explaining the geometry of the different types of compound eyes found in nature. Then, the recent approaches to bioinspired compound eye imaging systems with planar or curved designs are discussed in terms of materials, design layouts, integration schemes, and operating principles. Finally, the theoretical background, fabrication procedure, and design guidelines for biomimetic antireflective nanostructures, known as moth eye structures, are reviewed.

## Geometry of compound eyes in nature

Compound eyes, which can be found in arthropods (i.e., insects and crustaceans), are comprised of multiple lenses per eye, whereas camera-type eyes have a single lens. [Figure 1](#) presents the five distinct types of compound eyes in nature. These eyes are divided into two main classes: apposition compound eyes ([Figure 1\(a\)](#)) and superposition compound eyes ([Figures 1\(b\)–\(e\)](#)). In apposition eyes, each microlens-photoreceptor unit (i.e., ommatidium) is optically isolated from its neighbors. Each ommatidium has a single positive microlens that produces an image of a relatively large sector of the environment. The rhabdom, which measures the light intensity, has a narrow FOV and its role in imaging resembles a single rod in the camera-type eye. The principle focusing element is the crystalline cone, which is positioned between the microlens and rhabdom. The corneal lens provides only a minor focusing strength. Black screening pigments form opaque walls between adjacent ommatidia in order to avoid stray light. Apposition eyes have from hundreds up to tens of thousands ommatidia packed in non-uniform hexagonal arrays. The arrangement of ommatidia on a spherical shell allows apposition compound eyes to have an extremely wide FOV while the total volume consumption remains small (8).

The superposition compound eye has optically cooperating ommatidia, so that a bright image is produced by the combined action of many identical units. This type of eye has primarily evolved in nocturnal insects and deepwater crustaceans. The light from multiple facets combines on the surface of the photoreceptor layer to form a single erect image of an object. In neural superposition eyes ([Figure 1\(b\)](#)), the rhadoms are split into seven separate light guides, each with its own optical axis. Combined, the six summed signals and the seventh single produce an overall neural image in the eye that does not differ in principle from

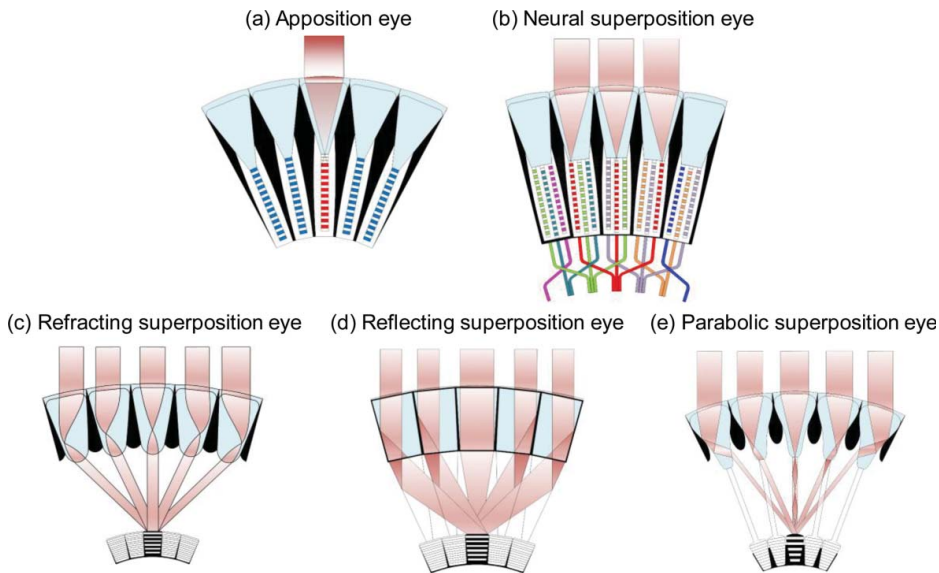


**Figure 1.** Illustrations of the five compound eye types in insects. (a) Apposition eyes achieve a high resolution because each ommatidium captures different visual fields. (b) Neural superposition eyes have a high resolution while increasing their sensitivity through integrating visual information from different input channels. Optical superposition eyes are composed of the (c) refracting, (d) reflecting, and (e) parabolic superposition eyes, which is a combination of refractive and reflective types. These eye types possess high sensitivity but sacrifice resolution.

that of the other compound eye. This provides redundant sampling and increased photosensitivity and minimizes the loss of visual acuity (1, 2).

In refractive superposition eyes (Figure 1(c)), light is refracted through multiple ommatidial lenses and is focused on a small portion of a common photoreceptor. Between the lenses and photoreceptors, there is a section of unpigmented and transparent cells that enable the photons to be shared efficiently from the adjacent ommatidia. The refractive superposition eye demonstrates improved photosensitivity by as much as three orders of magnitude compared with simple eyes. The number of arthropod groups with refracting superposition eyes is large: moths, beetles, and crustaceans such as krill are included. Another variant is the reflecting superposition eye (Figure 1(d)) found in decapod crustaceans, such as shrimp and lobsters. The facets of reflecting compound eyes have long rectangular walls, which function as biological mirrors that reflect light to the retina. In these eyes, a superposition image can be formed without lenses. The last example is the parabolic superposition eye (Figure 1(e)) found in many crabs and some mayflies. This structure involves ordinary lenses, cylindrical lenses, parabolic mirrors, and light guides. The mechanism of parabolic superposition eyes is the most complicated and relies on both reflection and refraction. Detailed optical systems and operating principles can be found in the existing literature (1, 2, 4, 7, 9–11).

Many insects have additional nanophotonic structures on the surface of their corneal microlenses (12), which are commonly called “nipple arrays” or “moth eye structures.” Figure 2 presents a scanning electron microscope (SEM) image of a compound eye in a nymphalid butterfly with three different magnifications (13). The nanostructures are closely packed and

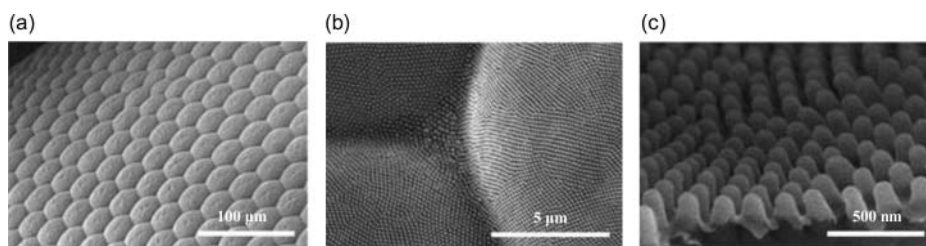


**Figure 2.** Compound eyes in a nymphalid butterfly, as revealed using a scanning electron microscope (SEM): (a) the complete eye, (b) the nipple arrays in one facet lens, and (c) a detailed view of the highly ordered nipple arrays. (Reproduced from (13) with permission of The Royal Society of Chemistry.)

uniformly distributed on the surface of the facet with a height of approximately 150 nm and a period of approximately 150 nm, which are significantly smaller than the wavelengths of visible light. These nanostructures are narrower at the top and wider at the bottom. These sub-wavelength tapered structures produce a gradual change of the refractive index, which reduces the light reflections at the surface. This improves the optical efficiency of compound eyes in low-light conditions. The theoretical background and artificial nanostructures for optical device applications are discussed in section “Biomimetic antireflective nanostructures.”

## Artificial insect eyes

### Planar-type insect eye imaging systems

Artificial implementation of compound eyes has attracted significant research interest due to their exceptionally wide FOV, high sensitivity to motion, and nearly infinite depth-of-field, which exhibits substantial potential for medical, industrial, and military applications (14–16). The use of miniaturized arrayed optical components fabricated using semiconductor planar processing technologies has been proposed to mimic natural compound eyes. Because commercially available image sensors such as CCD or CMOS are fabricated on planar wafers, a thin monolithic objective based on the compound eye concept must also be a planar structure.

Various technical approaches have been reported for planar-type compound eye imaging systems. Duparre et al. reported an artificial apposition compound eye, which consists of a microlens array (MLA) positioned on a substrate, with optical isolation of the channels, and an optoelectronic detector array (Figure 3) (17). The MLAs have a diameter ( $D$ ), focal length ( $f$ ), and pitch ( $p_L$ ), as illustrated in Figure 3(b). Pinhole arrays with a diameter ( $d$ ) and pitch ( $p_P$ ) are positioned in the microlens focal planes on the spacing structure's backside. The pitch difference enables different viewing directions for each optical channel. Each channel's optical axis points in a different direction in the object space with the optical axes of the channels directed outward if the pitch of the receptor array is smaller than that of the MLA. If the pitch of the MLA is smaller than that of the receptor array, the image is inverted. A pinhole array can be used to narrow the photo-sensitive area of the detector pixels if they are not sufficiently small for the required resolution.

In a more complex approach, mimicking a superposition compound eye, a stack of three MLAs has been used, as depicted in Figure 4 (18). The lenses of the first array image

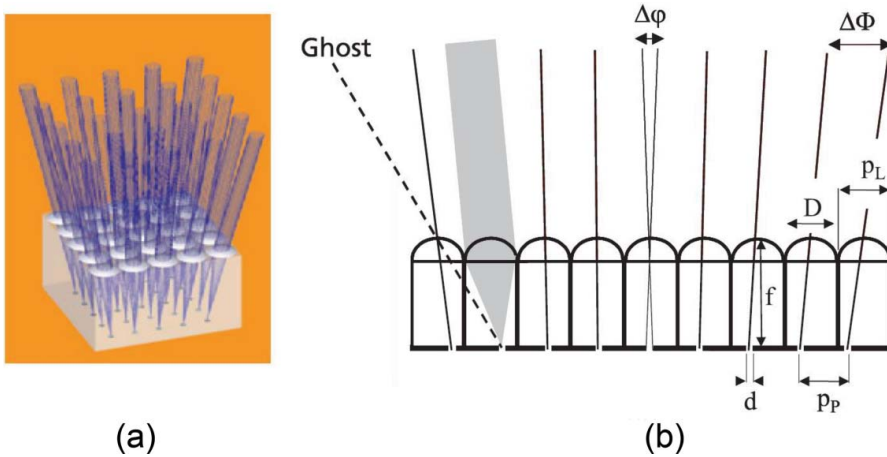


**Figure 3.** Schematic of a planar artificial apposition compound eye: (a) three-dimensional model of the artificial apposition compound eye displaying the focusing microlens array, and (b) cross-sectional view of (a) with the important parameters. (Reproduced with the permission from (17). © IOP Publishing. All rights reserved.)

demagnify and invert subimages of the object into the plane of the second lens array. The lenses of the third array image these inverted subimages to the image sensor plane. The lenses of the second array serve as field lenses, imaging the pupil of the first array to the corresponding entrance pupils of the third lens array. As depicted in Figure 4(a), the size, focal length, and distances in the system are optimized in order to obtain the correct superposition of the individual subimages in the plane of the image sensor. The parallel transfer of the different parts of an overall FOV with strong demagnification through separated optical

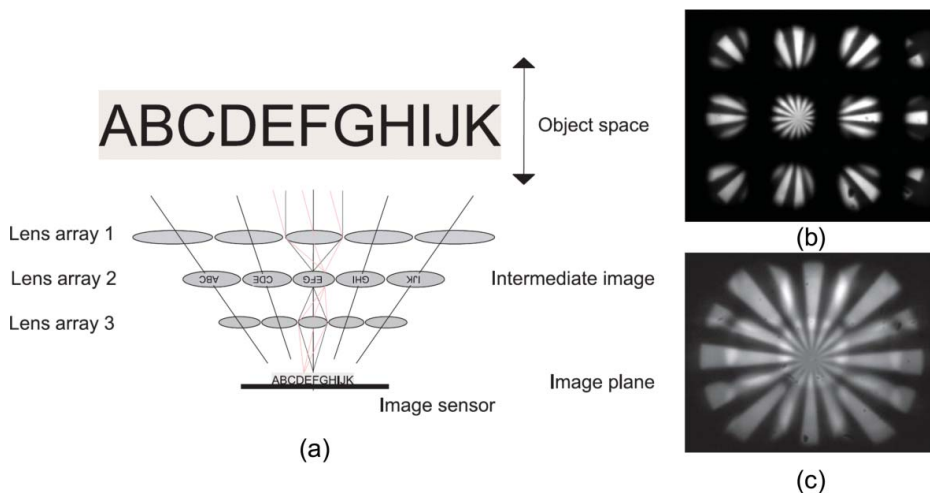


**Figure 4.** (a) Superposition-type compound eye imaging systems consisting of three layers of microlens arrays; (b) image of a radial star test pattern at an object distance of 41 cm from the compound eye; and (c) image captured at the image plane 120 mm from the compound eye. (Reproduced from (18) with the permission of the Optical Society of America.)

channels allows the superposition eye to have a collective space bandwidth product (SBP) that is equal to the sum of the individual channels' SBP. Consequently, the superposition eye has potential for significantly higher resolution than the experimentally demonstrated artificial apposition compound eyes.

Figures 4(b) and (c) are images of a radial star pattern captured at different axial positions from the superposition eye. It can be observed that matching the image plane of the individual telescopes to the position of perfect annexation of the partial images is critical. This is primarily influenced by the correspondence of the axial position of the intermediate images to the position of the field apertures. It is demonstrated that one overall image is generated through the transfer of different image sections through separated channels with strong demagnification. One drawback is the complexity of the lens configuration, which is much higher compared with the apposition compound eye. Future applications include large-object field microscopes. If it becomes possible to build ultrathin flexible cameras, a large range of products will be possible.

### ***Hemispherical compound eye lens arrays and optical components***

Because the above-mentioned imaging systems are fabricated on planar substrates, achieving a wide FOV in those structures is hindered due to the inherent flatness of the arrayed optical components. Several research groups have attempted to demonstrate MLAs on hemispherical or curved surfaces. One technique to create compound eye lens structures is irreversible thermomechanical deformation to form a curved MLA (19). A planar array of concave silica microlenses was fabricated using femtosecond laser pulses followed by HF treatment, as depicted in Figure 5. Then, silica was used as a mold to form a planar array of convex lenses using polymethyl methacrylate. Next, the array was heated and bent around a glass hemisphere. The resulting array demonstrates a  $140^\circ$  FOV, which is a significant improvement over planar lens arrays with FOVs of approximately  $90^\circ$ . With these techniques, faithful three-dimensional structures can be fabricated in a range of materials, which provides flexibility in material choice.

A more advanced example of the artificial compound eyes is a hemispherical polymer dome with a set of artificial ommatidia, which consist of a refractive polymer microlens, a light-guiding polymer cone, and a self-aligned waveguide to collect light with a small angular acceptance, as depicted in Figure 6(a) (20). The ommatidia are omnidirectionally arranged along a hemispherical surface such that they provide a wide FOV similar to that of natural compound eyes. The spherical configuration of the microlenses is achieved through reconfigurable microtemplating that enables polymer replication using a deformed elastomer membrane with microlens patterns. More importantly, the formation of polymer waveguides and cuvette-shaped cones, which are self-aligned with the microlenses, is also realized using a self-writing process in a photosensitive polymer resin. This 3D polymer optical system has potential for a broad range of optical applications, such as data storage, medical diagnostics, surveillance imaging, and light-field photography.

Another approach was used to create a dome structure smaller than an actual insect eye using a self-assembly method (Figure 6(b)). First, glass marbles with sizes of hundreds of nanometers were dispersed in water: then, an oil droplet with a uniform size of tens of micrometers was added. If the balance of the surface chemical energy between the water, oil, and glass marbles is maintained, the glass marbles migrate to the boundary between the



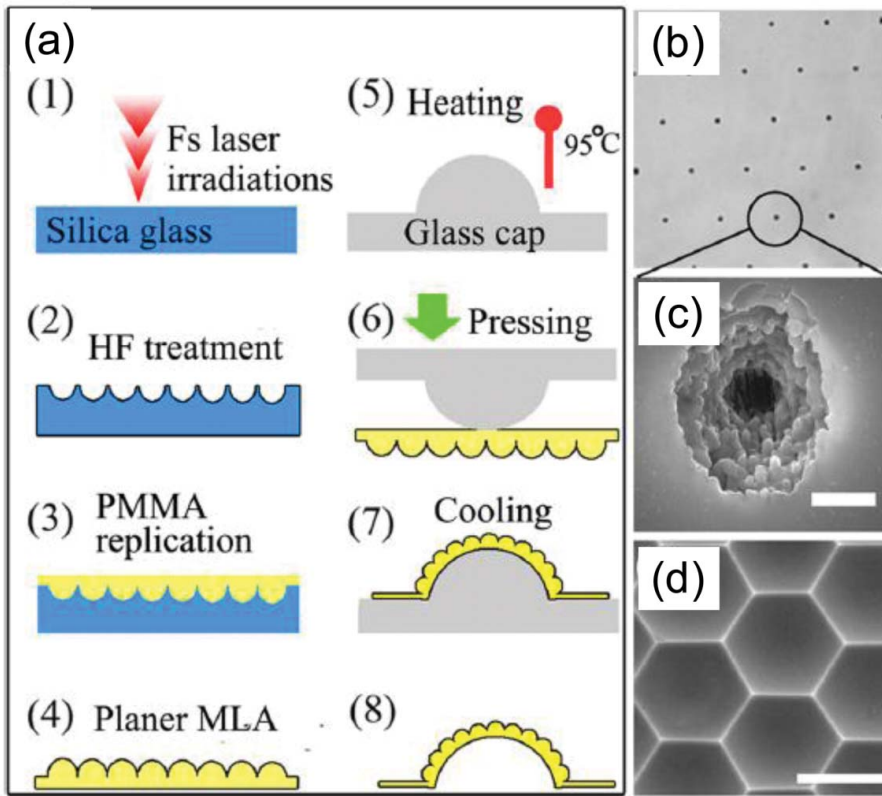


**Figure 5.** (a) Schematic of the fabrication process steps for microlens arrays on a hemispherical surface; (b) optical image of the laser exposure spots on a glass substrate; (c) SEM image of a single exposure spot; and (d) SEM image of the morphology of the lens array template. (Reprinted from (19), with the permission of AIP Publishing.)

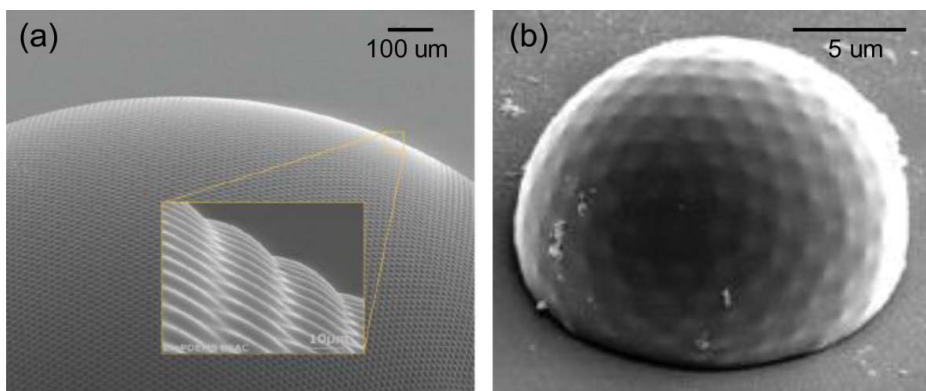


**Figure 6.** (a) SEM image of an artificial compound eye fabricated using the biologically inspired 3D optical synthesis method; (From (20). Reprinted with permission from AAAS.) and (b) SEM image of the dome patterns with 2D crystals on the hemispherical surfaces. (Reproduced from (21) with the permission of John Wiley & Sons, Inc.)



water and oil. The mixture of water-glass-oil droplets was placed on a board; then, the oil droplet transforms into a dome-shaped hemisphere. The glass marble lens automatically arranges itself into a dense, closely packed, hexagonal structure on the surface of the oil droplet. Finally, ultraviolet rays are projected onto the oil droplets and solidified the oil droplet to create a subminiature compound eye structure. Recently, eminently ordered and high-resolution MLA have been reported based on this self-assembly method (21, 22).

### ***Curved image sensors and hemispherical compound eye imaging systems***

A challenge in building digital cameras with the hemispherical compound apposition layouts of arthropod eyes is that the essential design requirements cannot be met using the existing planar sensor technologies or conventional optics. Recently, as a natural extension of recent advances in stretchable electronics and hemispherical photodetector arrays, Song et al. demonstrated arthropod-inspired cameras with nearly a full hemispherical shape with a  $160^\circ$  FOV (15). Their surfaces were densely populated by imaging elements (i.e., artificial ommatidia), which are comparable in number (180) to those of the eyes of fire ants and dark beetles (23, 24). The devices combined the elastomeric compound optical elements with the deformable arrays of thin silicon photodetectors into integrated sheets that could be elastically transformed from planar geometries to hemispherical shapes for integration into apposition cameras.

Figure 7(a) presents illustrations of an array of elastomeric microlenses and supporting posts joined by a base membrane (above) and a corresponding collection of silicon photodiodes and blocking diodes interconnected by serpentine-shaped wires and configured for matrix addressing (below). On the left of Figure 7(a), these two subsystems are depicted in planar geometries. The aligned bonding of these two subsystems places each photodiode at the focal position of a corresponding microlens in order to yield an integrated imaging system. Similar to the concept of a hemispherical polymer dome, the hydraulic actuation in a customized fluidic chamber can deterministically transform the planar layout into a full hemispherical shape without changes in the optical alignment or adverse effects on the electrical and optical performances. Figure 7(b) presents an image of a representative system after hemispherical deformation. A complete apposition-type compound eye camera consists of this imager combined with a perforated sheet of black silicon in order to prevent stray light. Through analogy with natural compound eyes, each microlens, supporting post, and photodiode corresponds to a corneal lens, crystalline cone, and rhabdom, respectively. The black perforated sheet functions as the black screening pigment, which can be found in apposition-type compound eyes. These device configurations appear to be applicable to other types of compound eyes, such as refracting/reflecting superposition eyes and neural superposition eyes.

Figure 8(a) depicts the operating principles of a hemispherical apposition compound eye camera through quantitative ray-tracing results for a simple  $8 \times 8$  ommatidia. Each microlens generates an image of the object with characteristics determined by the viewing angle. The overlap of a portion of each image with the active area of a corresponding photodiode generates a photocurrent at this location in the array. Improved resolutions can be realized through scanning the camera, as illustrated in the left frame of Figure 8(a). Figure 8(b) presents pictures, rendered on hemispherical surfaces, of soccer ball patterns captured at three different polar angles ( $-50^\circ$ ,  $0^\circ$ , and  $50^\circ$ ) relative to the center of the camera. This is

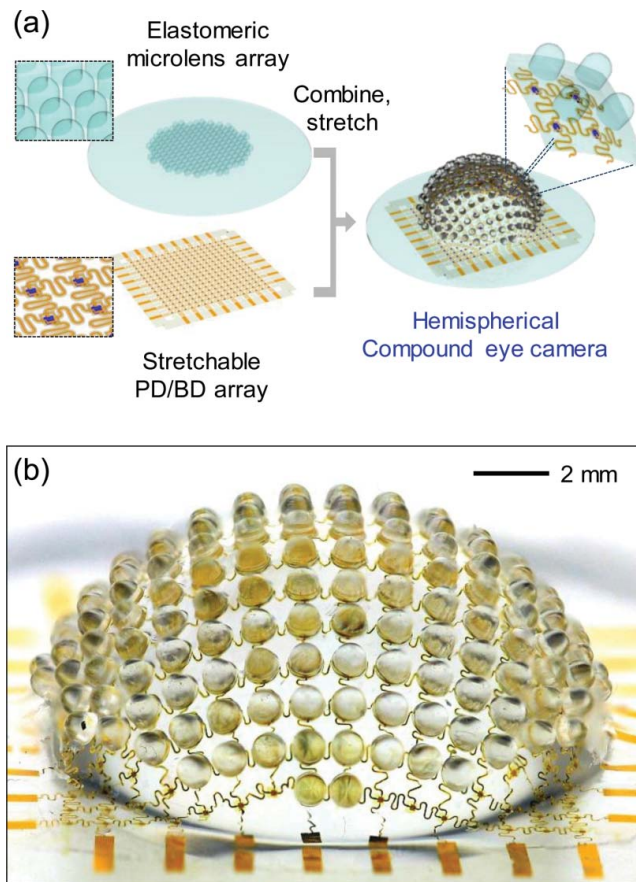


**Figure 7.** (a) Schematic of the integration schemes for a digital camera that takes the form of a hemispherical apposition compound eye; and (b) image of a representative compound eye system after hemispherical deformation. (Reprinted by permission from Macmillan Publishers Ltd: Nature (15), copyright © 2013.)

the first demonstration of a compound eye imaging system that enables exceptionally wide-angle FOV, without off-axis aberrations. The three images reveal comparable clarity without blurring or aberrations. The researchers also presented the imaging results demonstrating the nearly infinite depth-of-field, which results from the short focal length of the microlens and the nature of image formation in compound eyes. One drawback of such compound eye imagers is their inferior spatial resolution compared with that of camera-type eyes. In order to overcome these limitations, Lee et al. recently proposed the COMPUtational compound EYE (COMPU-EYE), which is a new compound eye design that increases the acceptance angles and uses a modern digital signal processing technique (25). The proposed COMPU-EYE yielded a four-fold improvement in spatial resolution.

Another type of artificial compound eye that features a panoramic FOV in a very thin package has been developed (14). In this system, three separate planar array layers, i.e., microlenses, photodetectors, and electromechanical interconnects, were fabricated and integrated into a curved optical system. The MLAs were molded on a glass carrier, which focuses light precisely on the sensitive areas of a silicon-based photodetector layer. This layer

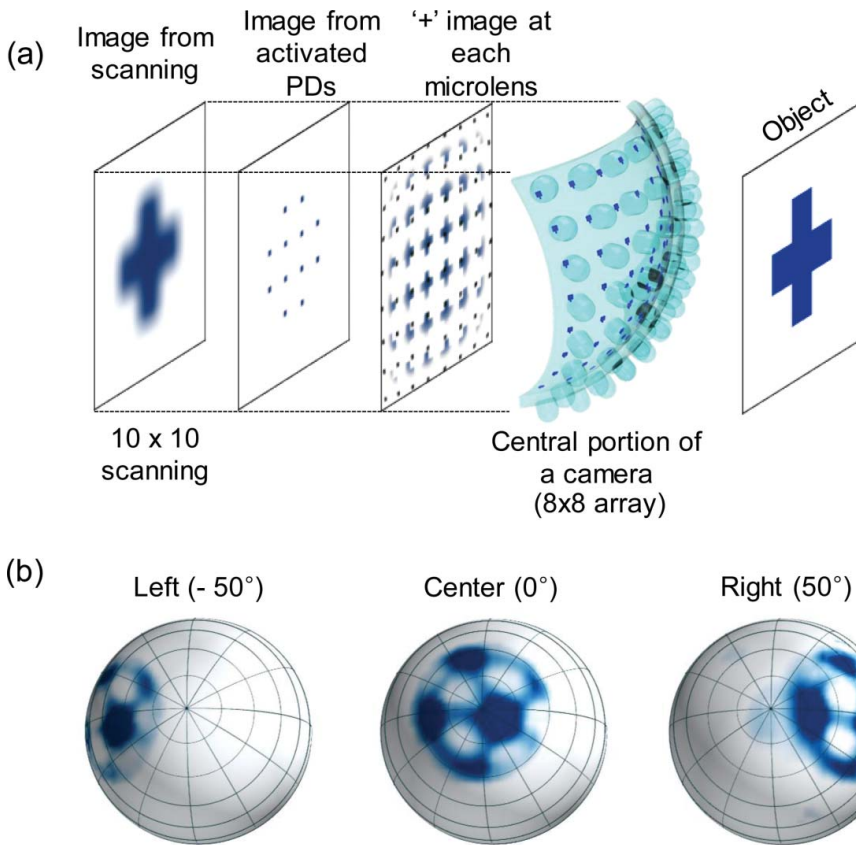


**Figure 8.** (a) Conceptual view of the image formation of a hemispherical apposition-type compound eye camera, and (b) pictures of a soccer ball captured at three different polar angles ( $-50^\circ$ ,  $0^\circ$ , and  $50^\circ$ ). Images are rendered on the hemispherical surface. (Reprinted by permission from Macmillan Publishers Ltd: Nature (15), copyright © 2013).

contains an array of analog very large-scale integration (VLSI) photodetectors as well as additional circuitry for signal processing. A flexible electromechanical interconnection layer, which was formed using a polyimide printed circuit board, physically supports the ensemble and transfers the output signals from the individual ommatidia to the processing units. These three individual layers were then aligned and integrated. The ommatidial layers were cut to the bottom layer using high-precision dicing. Because the interconnect layer is flexible, this step allows the entire array to be flexible and bendable. The final imager exhibited good hemispherical FOV ( $180^\circ \times 60^\circ$ ), high-temperature resistance, and local adaptation to illumination.

### Biomimetic antireflective nanostructures

The compound eyes in nocturnal insects present a fascinating object for biomimetic studies due to their well-organized hierarchical structures that consist of subwavelength structures (SWSs) with a tapered profile in the MLAs (26–28). The SWSs function as a homogeneous medium with a graded refractive index to reduce the Fresnel reflection at the surface, and

the MLAs focus the incident light toward the photoreceptor cells. When light is incident on the diffractive grating structures with a grating period ( $\Lambda$ ), the angles of the reflected/transmitted diffraction waves in the  $m$ th diffraction order are given by the grating equation, which is dependent on the period (Figure 9(a)). If the grating period becomes significantly smaller than the wavelength of the incident light, only the zeroth diffraction order is allowed to propagate. In this case, the structure behaves like an effective optical medium with an effective refractive index. The effective refractive index can be tailored to a selected quantity through adjusting the filling fraction of the grating structure. Figure 9(b) presents selected geometries of the SWSs and the corresponding index of refraction profiles. A simple binary grating translates into a single layer with a refractive index ( $n_{eff}$ ) between  $n_1$  and  $n_2$ , which depends on the filling fraction. For a multilevel surface relief profile, the effective media is film stacked with distinct levels of refractive indices. In the same way, a triangular grating is equivalent to optical media with a continuously graded refractive index. Hence, the design of such structures provides extremely low reflectance compared with that of conventional thin film stacks in broadband wavelength ranges.

Based on the effective medium theory and Fresnel reflection formulae, a taller height with a high packing density is desirable in order to enhance the antireflection properties in the broadband wavelength range. From this perspective, nanotip arrays with a tip height up to 1  $\mu\text{m}$  are ideal for broadband antireflection; however, it is evident that a taller height imposes a heavier burden on the fabrication procedure in various optical devices. Hence, it is important to determine the optimum geometry of the SWSs for a given height. Through observing the corneal nipple arrays of various butterfly species and reflectance calculations of three different types of SWSs, Stavenga et al. demonstrated that the parabola shape provides better antireflection properties than cone and Gaussian bell shapes. The parabola shape yields a nearly linear refractive index gradient, which is efficient in reducing the surface reflection.

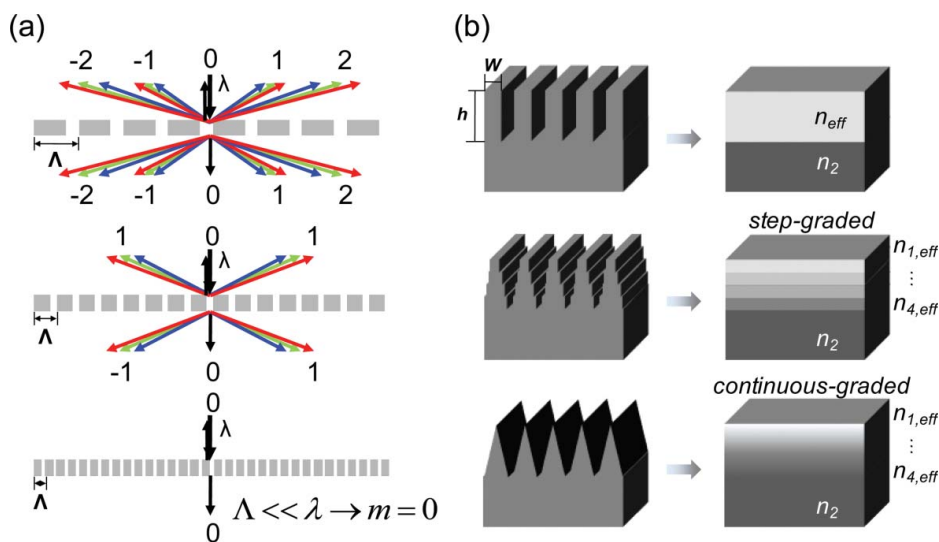


**Figure 9.** (a) Representation of simple binary gratings with three different grating periods. The  $m$ th order diffraction angle is determined by the grating period. (b) Illustration of different diffractive subwavelength structures and their thin film equivalents from effective medium theory.

Table 1. Fabrication methods of paraboloid and truncated structure.

Structure and fabrication method	Material	Ref.
<b>Paraboloid</b>		
Interference lithography, Inductively coupled plasma etching	Si, GaAs	[29–33]
Colloidal lithography, Reactive ion etching	Si	[34–36]
Nanoimprint lithography, Reactive ion etching	Si	[37–40]
Electron beam lithography, Fast atom beam/reactive ion etching	Si, SiO <sub>2</sub>	[41,42]
Hot embossing method	PVC	[43]
<b>Truncated paraboloid</b>		
Interference lithography, Inductively coupled plasma etching	GaAs	[33]
Colloidal lithography, Reactive ion etching	Si, SiO <sub>2</sub> , GaAs	[44–50]
Electron beam lithography, Inductively coupled plasma/reactive ion etching	InP, GaAs	[51]

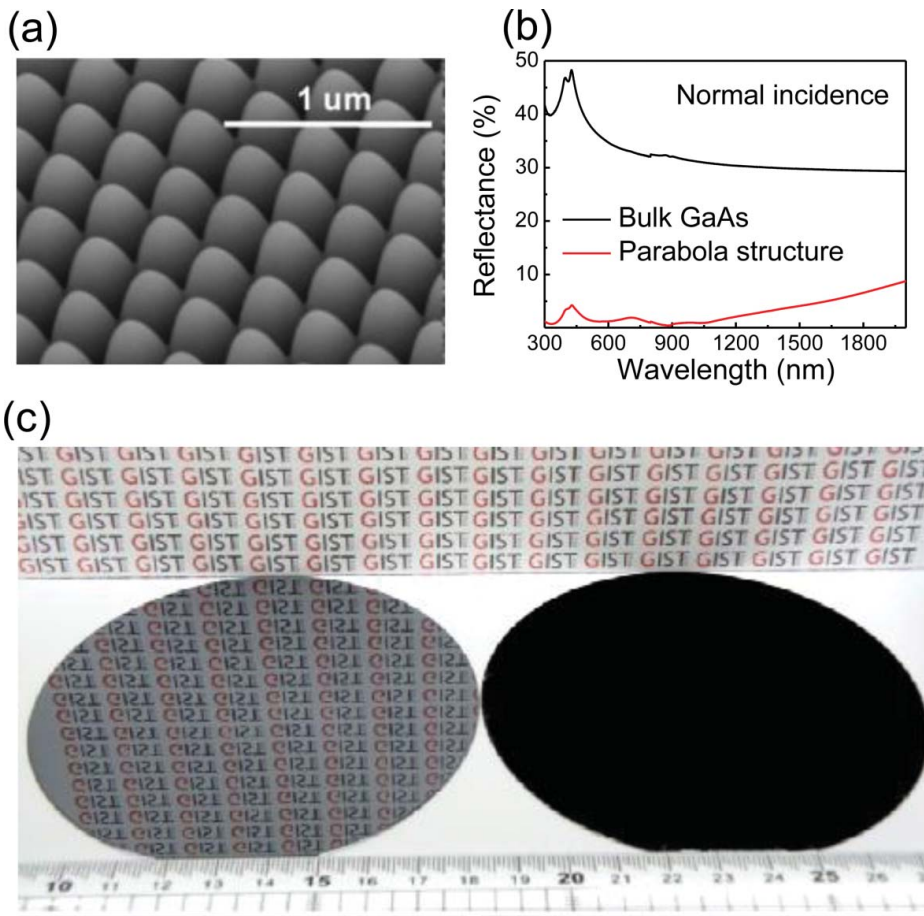


**Figure 10.** (a) SEM image of paraboloid-shaped nanostructures on a GaAs substrate fabricated via pattern transfer of lens-like shaped photoresists. (b) Measured reflectance as a function of wavelength for the fabricated paraboloid-shaped nanostructures on a GaAs substrate. The measured reflectance of the bulk GaAs is included for reference. (Reproduced from (30) with the permission of John Wiley & Sons, Inc.) (c) Comparison of 4" processed antireflective black silicon (right) with reflective polished bare silicon (left). (Reproduced from (51) with the permission of the Optical Society of America.)



In order to obtain SWSs with a tapered profile, many fabrication methods, such as electron-beam/interference lithography, nanoimprint lithography, metal nanoparticles, nanospheres or colloid formation, and Langmuir–Blodgett methods, have been utilized on various semiconductors and dielectric materials. The geometrical shape of the structures depends on the etching conditions and selection of etching gases. The degree of tapering in structures toward paraboloid or cone shapes can be normally adjusted through etching selectivity and undercut control. Truncated parabola structures, which can be useful for thin-film photovoltaic devices, have also been reported using similar methods. The diverse fabrication methods for parabola-shaped SWSs are summarized in Table 1 (29–51). Figure 10(a) presents the SEM image of the parabola SWSs fabricated on a GaAs substrate using simple process steps based on the combination of interference lithography, thermal reflow, and subsequent pattern transfer (52). The fabricated SWSs consist of parabolic grating patterns, thus resulting in a linearly graded index profile. It is also noted that the morphology of the etched surface is extremely smooth and the grating patterns are very uniform. As depicted in Figure 10(b), the SWSs on the GaAs substrate severely suppress the Fresnel reflection

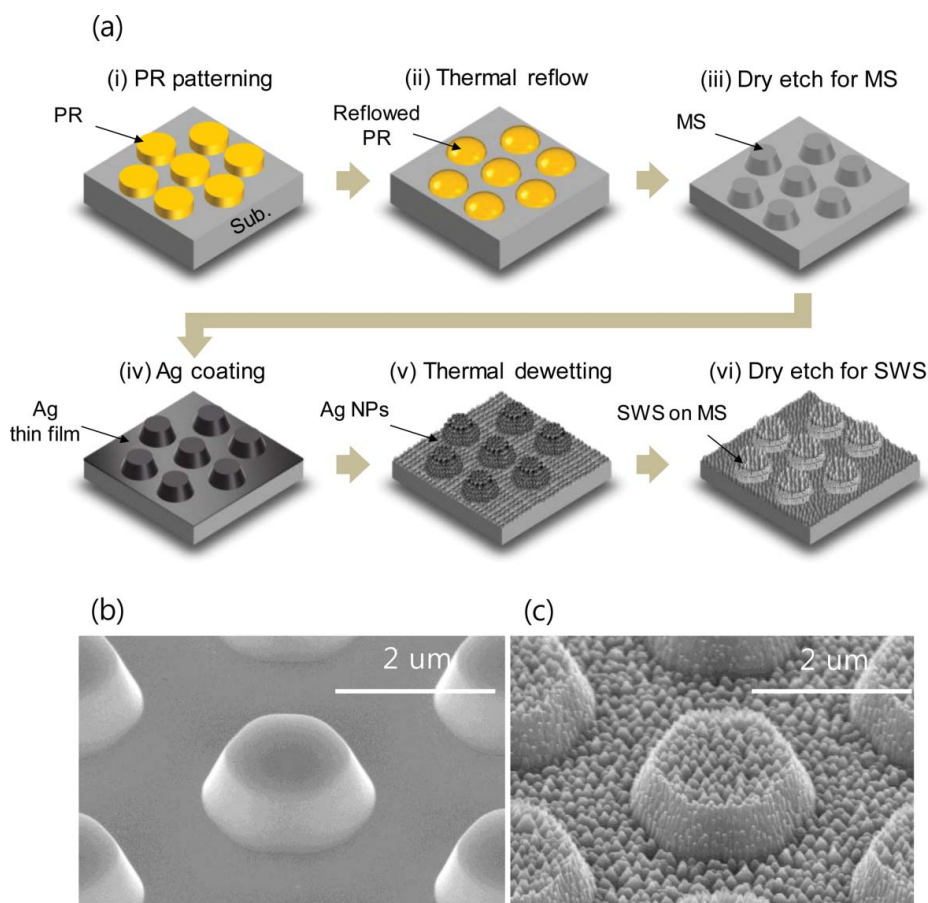


**Figure 11.** (a) Schematic of the fabrication procedure for the SWS/MS architecture. (b, c) Tilted-angle view of SEM images for the fabricated sample with (b) an MS and (c) an SWS/MS on a GaP substrate. (Reproduced by permission of The Optical Society of America (52).)



compared with that of the bulk GaAs substrate over broadband wavelength ranges. Several research groups have also reported the wafer-scale fabrication of SWSs for mass production purposes (Figure 10(c) from (53)). The uniform distribution of such SWSs with broadband antireflection characteristics over the surface of an entire wafer has potential to enhance device performance in various optoelectronic applications, such as solar cells (54, 55) and light-emitting diodes (56, 57). Also, the SWSs have a practical applicability in the field of flexible photodetectors suffering from a low optical efficiency.

The combination of microstructures and nanostructures yields micro-optic effects as well as low reflection. Song et al. demonstrated integrated ommatidium-like structures on semiconductor materials in order to enhance the optical efficiency in the optoelectronic devices (58). The fabrication procedure for these structures is depicted in Figure 11(a). First, hexagonally patterned microstructures (MSs) were fabricated on a gallium phosphide (GaP) substrate using a dry etch process with thermally reflowed photoresist (PR) masks (Figure 9(b)). For the SWS fabrication, Ag nanoparticles were grown on the entire surface via thermal dewetting of Ag thin films. These nanoparticles were used as an etch mask to define the tapered nanostructures on the micro-patterned substrate. The final nanostructures were randomly distributed on the MS arrays, with an average distance of 150 nm and a height of 120 nm (Figure 9(c)). The fabricated hierarchical microstructures and nanostructures exhibit minimized total internal reflection as well as Fresnel reflection. In recent years, the research on a hierarchical structure based on a flexible substrate polymer using a replica molding method have been reported (59–61). One of these papers demonstrated the efficiency improvement of a sheet-illumination display by using the bio-inspired hierarchical micro/nano structure, showing the possibility that biomimetic micro/nano structure that can be applied to various optoelectronic devices (61).

## Conclusion

In this review, the recent advances in mimicking compound eye imaging systems and nanophotonic structures were summarized. First, the basic anatomies and operating principles were explained for the five different types of compound eyes found in arthropods. The artificial compound eyes were categorized into three different types: planar compound eyes, hemispherical compound eye optics (without imagers), and hemispherical compound eyes. Examples of the three different types of artificial compound eyes illustrated the rapid progress of these concepts. In particular, it was demonstrated that the recent advances in flexible electronics enabled the realization of a complete set of well-matured, hemispherical compound eye imagers that incorporate all functional organs, such as cornea, crystalline cones, rhabdom, and screening pigments. The imaging characteristics of these compound eye sensors/imagers also illustrated the powerful mode of compound eye sensing concepts. The recent approaches to the development of artificial “moth eye” surfaces were also reviewed. Until now, the serpentine shape of electrode is needed in artificial compound eyes to resist the three-dimensional structural transformation, but it causes low pixel density. Also, the thickness of photosensitive cell should be thin to secure low modulus property. Thus, the size, resolution, and optical efficiency of artificial compound eyes remain not on the level of commercial products. However, future works will provide ideas for three-dimensional deformable electrodes, closed-packed curved image sensors, and photonic structures with enhanced optical efficiency.

## Funding

This work was supported by Basic Science Research Program of the National Research Foundation of Korea (NRF) (2014R1A1A1005945) and the Korea Basic Science Institute under the R&D program (D37615) supervised by the Ministry of Science, ICT and Future Planning.

## ORCID

Gil Ju Lee  <http://orcid.org/0000-0003-2225-2738>

## References

1. Mazzotta, G. M., and Costa, R. (2016) Circadian control of visual plasticity in arthropods. *Ethol. Ecol. Evol.* 28:1–19.
2. Katz, B., and Minke, B. (2009) Drosophila photoreceptors and signaling mechanisms. *Front. Cell. Neurosci.* 3(2):1–18.
3. Morante, J., and Desplan, C. (2005) Photoreceptor axons play hide and seek. *Nature Neurosci.* 8:401–402.
4. Land, M. F. (1997) Visual acuity in insects. *Annu. Rev. Entomol.* 42:147–177.
5. Marshall, J., Cronin, T. W., and Kleinlogel, S. (2007) Stomatopod eye structure and function: A review. *Arthropod Struct. Dev.* 36(4):420–448.
6. Land, M. F., and Nilsson, D. E. (2012) *Animal eyes*, 2nd ed. Oxford University Press, New York.
7. Land, M. F. (1988) The optics of animal eyes. *Contemp. Phys.* 29(1998):435–455.
8. Dudley, R. (2002) *The biomechanics of insect flight: Form, function, evolution*, 2nd ed. Princeton University Press, Princeton, NJ.
9. Land, M. F. (1980) Compound eyes: Old and new optical mechanisms. *Nature* 287:681–686.
10. Snyder, A. W. (1973) *Physics of vision in compound eyes*. Springer Publishing Company, New York.
11. Kirschfeld, K. (1976) *Neural principles in vision*. Springer Publishing Company, New York.
12. Parker, A. R., and Townley, H. E. (2007) Biomimetics of photonic nanostructures. *Nature Nanotech.* 2:347–353.
13. Doo-Hyun, K., Tumbleston, J. R., Henderson, K. J., Euliss, L. E., DeSimone, J. M., Lopez, R., et al. (2011) Biomimetic microlens array with antireflective “moth-eye” surface. *Soft Matter* 7:6404–6407.
14. Floreano, D., Pericet-Camara, R., Viollet, S., Ruffier, F., Bruckner, A., Leitel, R., et al. (2013) Miniature curved artificial compound eyes. *Proc. Natl. Acad. Sci.* 110(23):9267–9272.
15. Song, Y. M., Xie, Y., Malyarchuk, V., Xiao, J., Jung, I., Choi, K.-J. et al. (2013) Digital cameras with designs inspired by the arthropod eye. *Nature* 497:95–99.
16. Stollberg, K., Bruckner, A., Duparre, J., Dannberg, P., Brauer, A., and Tunnermann, A. (2009) The Gabor superlens as an alternative wafer-level camera approach inspired by superposition compound eyes of nocturnal insects. *Opt. Express* 17(18):15747–15759.
17. Duparre, J. W., and Wippermann, F. C. (2006) Micro-optical artificial compound eyes. *Bioinsp. Biomim.* 1:1–16.
18. Duparre, J. W., Schreiber, P., Matthes, A., Pshenay-Severin, E., Brauer, A., Tunnermann, A., et al. (2005) Microoptical telescope compound eye. *Opt. Express* 13(3):889–903.
19. Liu, H., Chen, F., Yang, Q., Qu, P., and He, S. (2012) Fabrication of bioinspired omnidirectional and gapless microlens array for wide field-of-view detections. *App. Phys. Lett.* 100(133701).
20. Lee, L. P., and Szema, R. (2005) Inspiration from biological optics for advanced photonic systems. *Science* 310:1148–1150.
21. Kuo, W.-K., Lin, S.-Y., Hsu, S.-W., and Yu, H. H. (2017) Fabrication and investigation of the bionic curved visual microlens array films. *Opt. Mater.* 66:630–639.
22. Serra, F., Gharbi, M. A., Luo, Y., Liu, I. B., Bade, N. D., Kamien, R. D., et al. (2015) Curvature-driven, one-step assembly of reconfigurable smectic liquid crystal “Compound Eye” lenses. *Adv. Optical Mater.* 3:1287–1292.

23. Kim, S. H., Kim, S.-H., and Yang, S.-M. (2009) Patterned polymeric domes with 3D and 2D embedded colloidal crystals using photocurable emulsion droplets. *Adv. Mater.* 23:3771–3775.
24. Wheeler, W. M. (1910) *Ants: Their structure, development and behavior*. Columbia University Press, New York.
25. Chapman, J. A. (1972) Ommatidia numbers and eyes in Scolytid beetles. *Ann. Entomol. Soc. Am.* 65:550–553.
26. Lee, W. B., Jang, H., Park, S., Song, Y. M., and Lee, H.-N. (2016) COMPU-EYE: A high resolution computational compound eye. *Opt. Express* 24(3):2013–2026.
27. Clapham, P. B., and Hutley, M. C. (1973) Reduction of lens reflexion by the “Moth Eye” principle. *Nature* 244:281–282.
28. Stavenga, D. G., Foletti, S., Palasantzas, G., and Arikawa, K. (2006) Light on the moth-eye corneal nipple array of butterflies. *Proc. Biol. Sci.* 273(1587):661–667.
29. Lee, K. C., Yu, Q., and Erb, U. (2016) Mesostucture of ordered corneal nano-nipple arrays: The role of 5–7 coordination defects. *Sci. Reports* 6(28342):1–11.
30. Song, Y. M., Yu, J. S., and Lee, Y. T. (2010) Antireflective submicrometer gratings on thin-film silicon solar cells for light-absorption enhancement. *Opt. Lett.* 35(3):276–278.
31. Leem, J. W., Song, Y. M., and Yu, J. S. (2011) Broadband wide-angle antireflection enhancement in AZO/Si shell/core subwavelength grating structures with hydrophobic surface for Si-based solar cells. *Opt. Express* 19(S5):A1155–A1164.
32. Song, Y. M., Jang, S. J., Yu, J. S., and Lee, Y. T. (2010) Bioinspired parabola subwavelength structures for improved broadband antireflection. *Small* 6(9):984–987.
33. Chen, X., Fan, Z.-C., Xu, Y., and Chen, L.-H. (2011) Microelectronic engineering fabrication of biomimic GaAs subwavelength grating structures for broadband and angular-independent antireflection. *Microelectron. Eng.* 88(9):2889–2893.
34. Leem, J. W., Song, Y. M., and Yu, J. S. (2011) Six-fold hexagonal symmetric nanostructures with various periodic shapes on GaAs substrates for efficient antireflection and hydrophobic properties. *Nanotechnology* 22(48):485304.
35. Zhu, J., Yu, Z., Burkhard, G. F., Hsu, C.-M., Connor, S. T., Xu, Y., et al. (2009) Optical absorption enhancement in amorphous silicon nanowire and nanocone arrays. *Nano Lett.* 9(1):279–289.
36. Chen, H. L., Chuang, S. Y., Lin, C. H., and Lin, Y. H. (2007) Using colloidal lithography to fabricate and optimize subwavelength pyramidal and honeycomb structures in solar cells. *Opt. Express* 15(22):14793–14803.
37. Zhang, X., Zhang, J., Ren, Z., Li, X., Zhu, D., Wang, T., et al. (2009) Morphology and wettability control of silicon cone arrays using colloidal lithography. *Langmuir* 25(13):7375–7382.
38. Asadollahbaik, A., Boden, S. A., Charlton, M. D. B., Payne, D. N. R., Cox, S., and Bagnall, D. M. (2014) Reflectance properties of silicon moth-eyes in response to variations in angle of incidence, polarisation and azimuth orientation. *Opt. Express* 22(S2):A402–A415.
39. Yu, Z., Gao, H., Wu, W., Ge, H., and Chou, S. Y. (2003) Fabrication of large area subwavelength antireflection structures on Si using trilayer resist nanoimprint lithography and liftoff. *J. Vac. Sci. Technol. B* 21(6):2874–2877.
40. Chen, Q., Hubbard, G., Shields, P. A., Liu, C., Allsopp, D. W. E., Wang, W. N., et al. (2009) Broadband motheye antireflection coatings fabricated by low-cost nanoimprinting. *Appl. Phys. Lett.* 94(26):263118.
41. Han, K.-S., Shin, J.-H., Yoon, W.-Y., and Lee, H. (2011) Enhanced performance of solar cells with anti-reflection layer fabricated by nano-imprint lithography. *Sol. Energy Mater. Sol. Cells* 95(1):288–291.
42. Kanamori, Y., Sasaki, M., and Hane, K. (1999) Broadband antireflection gratings fabricated upon silicon substrates. *Opt. Lett.* 24(20):1422–1424.
43. Toyota, H., Takahara, K., Okano, M., Yotsuya, T., and Kikuta, H. (2001) Fabrication of microcone array for antireflection structured surface using metal dotted pattern. *Jpn. J. Appl. Phys.* 40(7B):5–8.
44. Han, K. S., Lee, H., Kim, D., and Lee, H. (2009) Fabrication of anti-reflection structure on protective layer of solar cells by hot-embossing method. *Sol. Energy Mater. Sol. Cells* 93(8):1214–1217.

45. Sanatinia, R., Awan, K. M., Naureen, S., Anttu, N., Ebraert, E., and Anand, S. (2012) GaAs nanopillar arrays with suppressed broadband reflectance and high optical quality for photovoltaic applications. *Opt. Mater. Express* 2(11):1990–1995.
46. Xu, H., Lu, N., Qi, D., Hao, J., Gao, L., Zhang, B., et al. (2008) Biomimetic antireflective Si nanopillar arrays. *Small* 4(11):1972–1975.
47. Naureen, S., Sanatinia, R., Shahid, N., and Anand, S. (2011) High optical quality InP-based nanopillars fabricated by a top-down approach. *Nano Lett.* 11(11):4805–4811.
48. Li, Y., Zhang, J., Zhu, S., Dong, H., Jia, F., Wang, Z., et al. (2010) Bioinspired silica surfaces with near-infrared improved transmittance and superhydrophobicity by colloidal lithography. *Langmuir* 26(12):9842–9847.
49. Park, H., Shin, D., Kang, G., Baek, S., Kim, K., and Padilla, W. J. (2011) Broadband optical antireflection enhancement by integrating antireflective nanoislands with silicon nanoconical-frustum arrays. *Adv. Mater.* 23(48):5796–5800.
50. Zhang, X., Zhang, J., Ren, Z., Li, X., Zhang, X., Zhu, D., et al. (2009) Morphology and wettability control of silicon cone arrays using colloidal lithography. *Langmuir* 25(13):7375–7382.
51. Hsu, C.-M., Connor, S. T., Tang, M. X., and Cui, Y. (2008) Wafer-scale silicon nanopillars and nanocones by Langmuir-Blodgett assembly and etching. *Appl. Phys. Lett.* 93(13):33109.
52. Suemune, I., Nakajima, H., Liu, X., Odashima, S., Asano, T., Iijima, H., et al. (2013) Metal-coated semiconductor nanostructures and simulation of photon extraction and coupling to optical fibers for a solid-state single-photon source. *Nanotechnology* 24(45):455205.
53. Yeo, C. I., Song, Y. M., Jang, S. H., and Lee, Y. T. (2011) Wafer-scale broadband antireflective silicon fabricated by metal-assisted chemical etching using spin-coating Ag ink. *Opt. Express* 19 (55):A1109–A1116.
54. Leem, J. W., Guan, X.-Y., Choi, M., and Yu, J. S. (2015) Broadband and omnidirectional highly-transparent coverglass coated with bio-mimetic moth-eye nanopatterned polymer films for solar photovoltaic system applications. *Sol. Energ. Mat. Sol. Cells* 134:45–53.
55. Kang, S. M., Jang, S., Lee, J.-K., Yoon, J., Yoo, D.-E., Lee, J.-W., et al. (2016) Moth-eye TiO<sub>2</sub> layer for improving light harvesting efficiency in perovskite solar cells. *Small* 12(18):2443–2449.
56. Xiang, H.-Y., Li, Y.-Q., Zhou, L., Xie, H.-J., Li, C., Qu, Q.-D., et al. (2015) Outcoupling-enhanced flexible organic light-emitting diodes on ameliorated plastic substrate with built-in indium-tin-oxide-free transparent electrode. *ACS Nano* 9(7):7553–7562.
57. Wang, R., Xu, L.-H., Li, Y.-Q., Zhou, L., Li, C., Ou, Q.-D., et al. (2015) Broadband light out-coupling enhancement of flexible organic light-emitting diodes using biomimetic quasirandom nanostructures. *Adv. Optical Mater.* 3(2):203–210.
58. Song, Y. M., Park, G. C., Jang, S. J., Ha, J. H., Yu, J. S., and Lee, Y. T. (2011) Multifunctional light escaping architecture inspired by compound eye surface structures: From understanding to experimental demonstration. *Opt. Express* 19 (52):A157–A165.
59. Shao, J., Ding, Y., Wang, W., Mei, X., Zhai, H., Tian, H., et al. (2014) Generation of fully-covering hierarchical micro-/nano- structures by nanoimprinting and modified laser swelling. *Small* 10 (13):2595–2601.
60. Raut, H. K., Dinachali, S. S., Loke, Y. Ch., Ganesan, R., Ansha-Antwi, K. K., Gora, A., et al. (2015) Multiscale ommatidial arrays with broadband and omnidirectional antireflection and antifogging properties by sacrificial layer mediated nanoimprinting. *ACS Nano* 9(2):1305–1314.
61. Kwon, Y. W., Park, J., Kim, T., Kang, S. H., Kim, H., Shin, J., et al. (2016) Flexible near-field nanopatterning with ultrathin, conformal phase masks on nonplanar substrates for biomimetic hierarchical photonic structures. *ACS Nano* 10(4):4609–4617.